Received May 3, 2021, accepted May 14, 2021, date of publication May 20, 2021, date of current version May 27, 2021.

Digital Object Identifier 10.1109/ACCESS.2021.3082174

In Silico Investigation of CACNA2D1 S755T Mutation Associated With Short QT Syndrome

SHUGANG ZHANG[1,4], WEIGANG LU[2,4], FEI YANG[3], AND ZHIQIANG WEI[1]

[1]College of Information Science and Engineering, Ocean University of China, Qingdao 266100, China
[2]Department of Educational Technology, Ocean University of China, Qingdao 266100, China
[3]School of Mechanical, Electrical and Information Engineering, Shandong University, Weihai 264200, China
[4]Biological Physics Group, School of Physics and Astronomy, The University of Manchester, Manchester M13 9PL, U.K.

Corresponding author: Weigang Lu (luweigang@ouc.edu.cn)

This work was supported in part by the National Key Research and Development Program of China under Grant 2018YFB0204204, and in part by the Shandong Provincial Postdoctoral Program for Innovative Talents (grantee S. Zhang).

ABSTRACT Short QT syndrome (SQTS) is a genetic disease characterized by constantly short QT intervals and high risks of sudden death. SQTS6 is one of the identified SQTS genotype variants associated with the *CACNA2D1* S755T mutation. However, the pathogenesis of SQTS induced arrhythmias remains unclear. To identify the underlying mechanisms of SQTS6 induced arrhythmias, a multi-scale human ventricle model comprising cell to organ levels was built. Cellular data was fitted at the cell level to reproduce the electrophysiological alterations reported in experiments. The influences were further explored at tissue and organ levels using idealized strand or tissue sheet models, and realistic ventricular slice and three-dimensional organ models. Simulation results suggested that, at the cellular level, the action potential duration (APD) and the effective refractory period (ERP) of myocytes were significantly abbreviated in the mutation condition. The unevenly changed APD and ERP led to transmural heterogeneity remodeling, and resulted in decreased temporal vulnerability. In addition, the S755T mutation shortened the critical length for initiating reentrant spiral waves, which enhanced the spatial vulnerability and provided substrates for reentry arrhythmias. Regarding the sustainability of arrhythmias, the evoked spiral waves or scroll waves persisted in the mutation condition but did not persist in the wild-type condition. The present study clearly suggested that the *CACNA1DC* S755T mutation can facilitate the initiation and maintenance of ventricular arrhythmias, and therefore contributes to higher risks of ventricular arrhythmias in SQTS6 patients.

INDEX TERMS Inherited heart disease, short QT syndrome, simulation, ventricular arrhythmia.

I. INTRODUCTION

Short QT syndrome (SQTS) is a rare but dangerous inherited cardiac channelopathy characterized by marked shortened QT intervals, and is associated with an increased risk of abnormal heart rhythms and even sudden cardiac death (SCD) in individuals with a structurally normal heart. SQTS was first reported in 2000 [1], and since then great efforts have been made to unveil the genetic and cellular basis of SQTS. Up to now, totally eight SQTS genotype variants have been recognized [2] and are associated with gain-of-function mutations to K^+ channel genes (SQTS1-3) [3]–[7], loss-of-function mutations to Ca^{2+} channel genes (SQTS4-6) [8], [9], and mutations to other channel genes including Na^+ (SQTS7) [10] and anion exchanger (SQTS8) [11]. Among these variants, SQTS6 is caused by mutations to the *CACNA2D1* gene where a serine to threonine substitution occurred (i.e., p.Ser755Thr, or S755T). Due to that the *CACNA2D1* gene encodes the $Ca_v\alpha_2\delta-1$ subunit of the L-type calcium channel, the corresponding ionic current I_{CaL} is the major affected current. According to the experimental observations by Templin *et al.* [9], both the channel kinetics and the conductance of I_{CaL} could be changed in the mutation condition. In particular, small positive shifts of both activation and inactivation curves were found in those cells with the mutant $Ca_v\alpha_2\delta-1$ subunit, and the amplitude of I_{CaL} was significantly reduced by more than 70%.

L-type calcium channels are responsible for the excitation-contraction coupling of cardiac muscle, and play major roles in the plateau phase of cardiac action potential. The S755T

The associate editor coordinating the review of this manuscript and approving it for publication was Yang Tang.

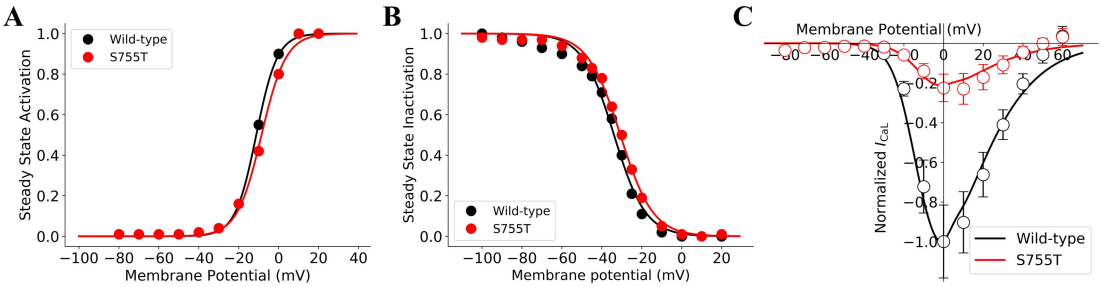

FIGURE 1. Fitting results for I_{CaL}. Dots, circles, and error bars are experimental data from [9], whereas the solid lines are the model fits. (A) Steady-state activation curves for wild-type (black) and S755T (red) conditions. (B) Steady-state inactivation curves. (C) Current-voltage (I-V) curves.

'loss-of-function' mutation will induce dysfunctions of I_{CaL} and then result in abnormal excitations of cardiomyocytes that finally lead to arrhythmias [12]–[14]. Though the molecular mechanisms for SQTS6 and the clinical electrocardiographic characteristics were well documented in Templin et al's study [9], there are yet no experimental studies on how the S755T mutation affects the propagation behaviour of excitation waves and provides substrates for ventricular arrhythmia.

In this study, an *in silico* investigation was conducted to reproduce the electrophysiological activities in the absence and presence of the *CACNA1DC* S755T mutation. By constructing a multi-scale virtual heart, we successfully expanded the molecular and subcellular alterations reported in previous studies to the tissue and organ levels. Simulation results on these higher levels comprehensively unveiled the arrhythmogenic substrate in SQTS6, and provided possible pathological links between the *CACNA1DC* S755T mutation and ventricular arrhythmias.

II. METHODS

A. FITTING I_{CaL} OF WILD-TYPE AND CACNA2D1 S755T MUTATION

The L-type calcium current in the TNNP06 model [15] was calculated as:

$$I_{\mathrm{Cal}} = g_{\mathrm{Cal}} d f f_2 f_{\mathrm{CaSS}} 4 \times \frac{(V-15)F^2}{RT} \frac{0.25\mathrm{Ca}_{\mathrm{SS}} e^{2(V-15)F/RT} - \mathrm{Ca}_{\circ}}{e^{2(V-15)F/RT} - 1} \quad (1)$$

where g_{CaL} is the maximum I_{CaL} conductance. d is the activation gate, f_1 and f_2 are the slow and fast voltage inactivation gates respectively. F represents the Faraday's constant, R is the ideal gas constant, and T is the temperature in kelvins. $\mathrm{Ca_i}$ and $\mathrm{Ca_o}$ are separately the intracellular and extracellular Ca^{2+} concentrations.

The steady-state activation curves in the wild-type and the *CACNA2D1* S755T mutation conditions were fitted using the following Boltzmann equations:

$$d_{\infty,\mathrm{WT}} = \frac{1}{1 + e^{2(-11.19-V)/5.26}} \quad (2)$$

$$d_{\infty,\mathrm{S755T}} = \frac{1}{1 + e^{2(-8.56-V)/6.12}} \quad (3)$$

Also, the steady-state inactivation curves were fitted using:

$$f_{\infty,\mathrm{WT}} = \frac{1}{1 + e^{(V+33.90)/7.89}} \quad (4)$$

$$f_{\infty,\mathrm{S755T}} = \frac{1}{1 + e^{(V+30.72)/8.15}} \quad (5)$$

In the wild-type cell model, a scaling factor of 0.838 was applied to g_{CaL} to achieve the same I_{CaL} amplitude in the baseline model. The scaled g_{CaL} was further downregulated by 0.77 to fit the I-V curve and reproduce the effects of S755T mutation on I_{CaL}. Fig. 1 presents the voltage dependence of the fitted I_{CaL} together with the experimental data, demonstrating a good agreement between simulation and experimental results.

B. SINGLE CELL SIMULATION

The Ten Tusscher *et al.* biophysically detailed model (TNNP06 model) [15] for human ventricular action potential was used in this study. The changes of cell membrane potential were described using:

$$\frac{\partial V}{\partial t} = \frac{(I_{\mathrm{ion}} + I_{\mathrm{stim}})}{C_{\mathrm{m}}} \quad (6)$$

I_{ion} and I_{stim} are separately the total ion channel current and stimulus current. C_{m} is the membrane capacitance.

The modified I_{CaL} for wild-type and *CACNA2D1* S755T mutation conditions was incorporated into the TNNP06 model. The same I_{CaL} was used in all three cell types, i.e., no transmural heterogeneity of the I_{CaL} depression in mutation conditions was considered. Action potentials were evoked by a series of supra-threshold stimuli with an amplitude of 52 pA/pF and duration of 1 ms. The basic cycle length was 800 ms that corresponds to the normal heart rate 75 per minute. Fifty stimuli (S1) were applied to the cell model to achieve its steady state. The last AP were recorded for measuring APD, AP overshoot, maximum upstroke velocity, and resting membrane potential.

The effective refractory period (ERP) was measured using the S1-S2 protocol consisting of 50 S1 stimuli and an S2 stimulus. The S1 stimuli were applied at a frequency of 1.25 Hz

with an amplitude of 52 pA/pF and duration of 1 ms. The premature stimulus S2 that had the same amplitude and duration as S1, was applied at some diastolic intervals after the AP evoked by the last S1 stimulus. The ERP was measured as the smallest diastolic interval for which the overshoot of the S2-evoked AP reached 80% of that induced by the S1 stimulus [16].

C. MULTI-SCALE TISSUE MODELS FOR HUMAN VENTRICLES

The tissue models for simulating action potential propagation were described using the monodomain equation [17]:

$$\frac{\partial V}{\partial t} = \nabla \cdot \mathbf{D} - (\nabla V)\frac{(I_{\text{ion}} + I_{\text{stim}})}{C_{\text{m}}} \tag{7}$$

where $\mathbf{D}$ is the diffusion coefficient tensor for describing the intercellular electrical coupling via gap junctions.

For one-dimensional (1D) simulation, a 15 mm long transmural 1D strand with 100 nodes was constructed. The strand length was set to 15 mm to be consistent with the normal range of human transmural ventricle width (4∼14 mm) in previous studies [18], [19]. The proportions for transmural cell types were 25:35:45 for ENDO, MID, and EPI cells, which were identical to previous studies [20]. The isotropic coefficient was set to 0.154 mm^2/ms to get a conduction velocity of 71.9 cm/s, which is very close to the 70 cm/s that recorded in the human myocardium [21].

For the idealized two-dimensional (2D) simulations, the 1D strand was expanded in the y direction to form a 15×60 mm^2 tissue sheet. Isotropic cell-to-cell coupling was assumed in the idealized model, and the isotropic coefficient was kept the same as in the 1D strand. For the realistic 2D ventricle tissue slice, the $\mathbf{D}$ was anisotropic and the coefficients along and perpendicular to the fiber orientation were set to 0.154 and 0.0385 mm^2/ms respectively. For the realistic three-dimensional (3D) bi-ventricle geometry, the anisotropic coefficients were the same as in the 2D realistic tissue slice.

D. NUMERICAL DETAILS

The differential equations for the membrane potential and the gating variables were solved by the Forward Euler method with a time step of 0.02 ms. The spatial resolution was 0.15 mm in the 1D strand and the idealized 2D tissue sheet. For the realistic 2D ventricular slice and the 3D bi-ventricle simulations, the spatial resolution was 0.2 mm kept from the geometry reconstructed from DT-MRI [22], [23]. Neumann boundary conditions with zero-flux were implemented at geometry boundaries [24].

For the computations of the 1D strand and the idealized 2D sheet models, OpenMP [25] was used for parallelization. For the computations of the realistic 2D and 3D models, the optimized GPU algorithm proposed in [26] was used.

E. MEASUREMENT OF VULNERABLE WINDOW IN 1D STRAND: THE TEMPORAL VULNERABILITY

The temporal vulnerability to the unidirectional conduction block was investigated using the 1D strand model. For any location on the strand, a premature stimulus (S2) applied to the refractory tail of a previous excitation wave (S1) could induce the unidirectional block. The exact time window when the unidirectional conduction block happened was recorded as a *vulnerable window* (VW). The strength and duration of the S1 stimulus was applied to the first 0.45 mm segment in the endocardial side. The S2 stimulus was also applied to a 0.45 mm long segment on the strand.

F. CRITICAL SUBSTRATES TO INITIATE REENTRY IN 2D SHEET: THE SPATIAL VULNERABILITY

The spatial vulnerability to reentry arrhythmia was investigated using the 2D tissue sheet. The formation of spiral waves needed not only the strict time window (i.e., vulnerable window) that the premature stimulus occurs, but also a minimum stimulus size for spiral waves to survive. The minimum stimulus size was defined as *critical size*, and its height was named *critical length* if the width is fixed. The S1 stimulus was applied to the area on the endocardial side of the sheet to initiate a planar wave, and the S2 stimulus was applied to a local epicardial region during the vulnerable window to evoke the unidirectional propagation that can lead to reentry.

G. INITIATION OF REENTRY IN THE ANATOMICAL 2D VENTRICULAR SLICE AND 3D VENTRICLE

In the anatomical 2D slice, the S1 stimuli were applied on multiple sites of endocardium as previous studies [27] to reproduce the activation pattern observed in [28]. The spiral wave was also evoked by a premature stimulus S2, which was applied on a local area of the left epicardium during the vulnerable window.

III. RESULTS

A. SIMULATION OF I_{CaL} IN WILD-TYPE AND CACNA2D1 S755T MUTATION CONDITIONS

The steady-state activation and inactivation curves for wild-type and *CACNA2D1* S755T mutation conditions are shown in Fig. 1. As observed in the figure, both activation and inactivation curves of S755T showed slight positive shifts (towards depolarization). Beside the channel kinetics, the S755T mutation largely reduced the L-type calcium channel conductance. Resulted current-voltage curves (I-V curves) are plotted in Fig. 1C.

B. SIMULATION OF ACTION POTENTIALS IN WILD-TYPE AND CACNA2D1 S755T MUTATION CONDITIONS

Changes of action potential characteristics in the *CACNA2D1* S755T mutation myocytes were simulated using the Tusscher-Noble-Noble-Panfilov (TNNP06) model with the modified I_{CaL}. Steady-state action potentials for the endocardial (ENDO), middle (MID/MCELL), and epicardial (EPI)

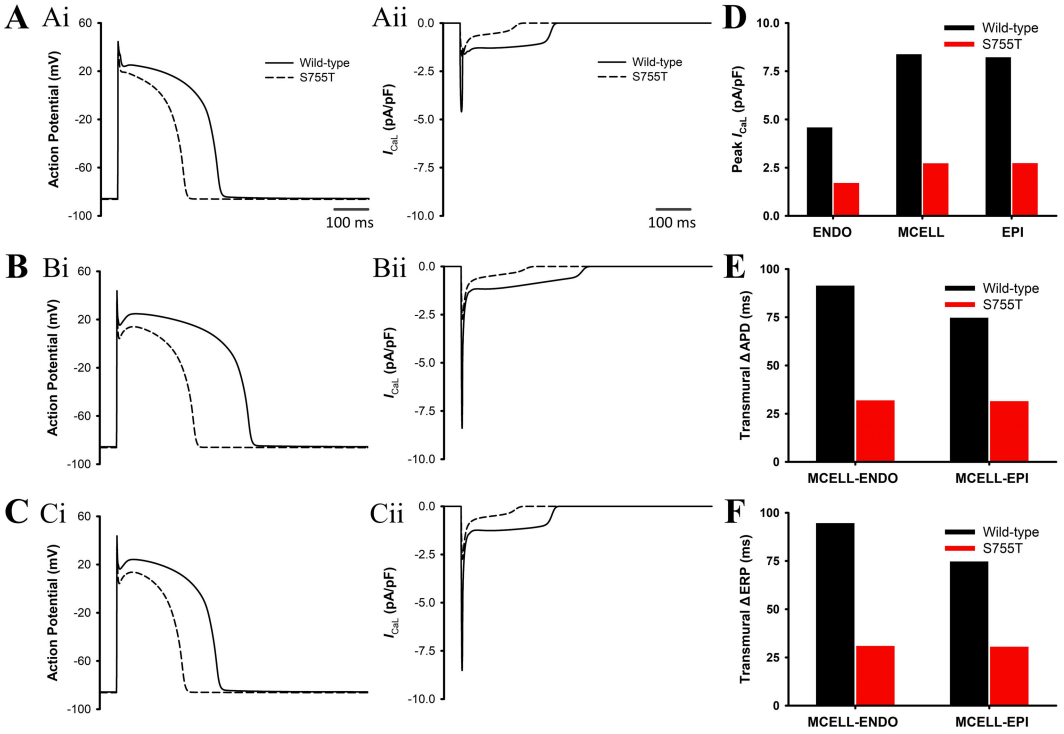

FIGURE 2. Simulation of action potentials and I_{CaL} time courses. (A) Steady-state (1.25 Hz) action potentials (Ai) and the corresponding I_{CaL} (Aii) for EPI cells. Solid and dashed lines represent wild-type and S755T conditions respectively. (B) Steady-state action potentials (Bi) and the corresponding I_{CaL} (Bii) for MIDDLE cells. (C) Steady-state action potentials (Ci) and the corresponding I_{CaL} (Cii) for ENDO cells. (D) Peak amplitude of I_{CaL} of three cell types in wild-type and S755T conditions. (E) Transmural APD difference between ENDO and MID cells, and between EPI and MID cells in wild-type and S755T conditions. (F) Transmural ERP differences in wild-type and S755T conditions.

TABLE 1. Action potential properties for Wild-Type and S755T conditions.

	Wild-type			*CACNA2D1 S755T*		
	EPI	**ENDO**	**MID**	**EPI**	**ENDO**	**MID**
APD_{25}	197.30	192.56	261.50	75.58 ↓↓	79.04 ↓↓	85.30 ↓↓
APD_{50}	272.20	271.28	358.86	164.30 ↓↓	165.00 ↓↓	193.56 ↓↓
APD_{90}	301.14	300.42	391.94	197.18 ↓↓	196.76 ↓↓	228.78 ↓↓
V_{rest}	-85.57	-85.59	-85.45	-86.18	-86.19	-86.16
dV/dt_{max}	392.72	393.64	392.66	416.79	417.08	417.14
Overshoot	41.81	42.90	41.98	43.42	44.28	43.52

myocytes at a pacing cycle length of 1.25 Hz were plotted in Fig. 2. As observed in the first column, action potentials of all three cell types were significantly abbreviated, with altered plateaus and accelerated repolarization courses. Among three types of myocytes, the MID cell experienced the largest reduction of APD that dropped by 163.2 ms whilst the other two types were 103.7 and 104 ms respectively. The abbreviation of APD was attributed to the decreased I_{CaL} in CACNA2D1 S755T cells, which was only thirty percent of that in the wild-type condition (see Fig. 2Aii-Cii for I_{CaL} courses and Fig. 2D for comparisons of the peak amplitude of I_{CaL}). Detailed AP characteristics are listed in Table 1.

The unevenly shortened APD also changed the transmural heterogeneity in the ventricular wall. Specifically, APD differences (ΔAPD) between ENDO and MID, and EPI and MID, were all decreased from more than 90 ms to about 30 ms. Transmural ERP differences (ΔERP) were also decreased by a similar extent. The comparisons of ΔAPD and ΔERP are plotted in Fig. 2 E&F.

C. INVESTIGATING THE VULNERABILITY TO REENTRY ARRHYTHMIA IN SQTS6 – 1D AND 2D SIMULATIONS

We first investigate the temporal vulnerability in the SQTS6 condition using a 15 mm long 1D strand model. Initiating reentry arrhythmia requires not only a premature stimulus, but also an appropriate time period within which the evoked excitation wave would propagate towards only one side before it degenerated into spiral waves. The unidirectional conduction block phenomenon can be simulated in the 1D strand (shown in Fig. 3A&B), and the time period

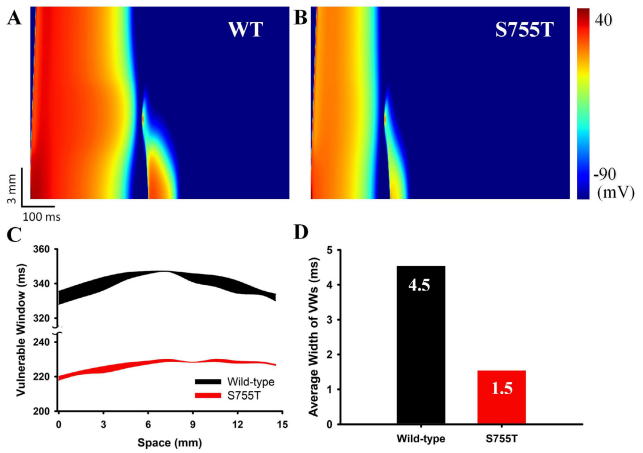

FIGURE 3. Simulation results of the vulnerable window in the 1D strand model. (A-B) Unidirectional conduction block in wild-type and *CACNA2D1* S755T mutation strands. (C) Distribution of vulnerable windows across the strand. Black and red belts stand separately for the wild-type and the S755T mutation conditions. (D) Comparison of the average width of VWs in the two conditions.

when such phenomenon occurs is defined as a *vulnerable window* (VW). The width of the vulnerable window is a rational indicator for the tissue's temporal vulnerability, since the wider VW makes premature stimuli more likely to evoke unidirectional conduction blocks and reentry arrhythmias. Fig. 3C plots the overall distribution of the VW across the 1D strand. The average width of VWs was decreased from 4.5 ms to 1.5 ms.

After the investigation of the temporal vulnerability, the transmural 1D strand model was expanded to an idealized 2D sheet model to explore the spatial vulnerability to reentry arrhythmia in SQTS6 condition. Spatial vulnerability can be quantified by measuring the minimum tissue size for a premature stimulus S2 to successfully initiate a spiral wave, which is defined as critical size. It can be further simplified by fixing the width of the S2 stimulating area and measuring critical length of it. Simulation results are demonstrated in Fig. 4. From the figure we can see that the measured critical length in the SQTS6 tissue was significantly shorter than that in the wild-type condition and was even less than half of its original length (15.4 mm vs. 35.7 mm), indicating highly increased chances to initiate reentry arrhythmias in the SQTS6 tissue.

D. INVESTIGATING THE SUSTAINABILITY OF REENTRY ARRHYTHMIA IN SQTS6 – 2D AND 3D SIMULATIONS USING REALISTIC GEOMETRIES

To further investigate the potential influences of the *CACNA2D1* S755T mutation on sustainability of reentry, simulations were conducted using realistic 2D and 3D geometries. The 2D simulation results of spiral waves in S755T mutation and wild-type conditions, evoked by a premature stimulus (S2) applied on a local area of the left epicardium, are shown in Fig. 5. It can be observed that spiral waves could be formulated in both cases, however, their lifespans were not the same. In the 2D tissue slice of the *CACNA2D1* S755T mutation, shown in Fig. 5A, the spiral wave evoked by S2 could keep spinning for more than 4 cycles. This type of reentry, named *functional reentry* that characterized by spinning around a functional core, lasted about half a second and then transformed to *anatomical reentry* that the excitation wave propagated through the reentrant circuit existed between left and right ventricles. The formulated anatomical reentry showed no sign of termination. In contrast, the evoked spiral wave in the wild-type tissue could barely sustain for 1 cycle before it drifted out of the epicardial boundary, with a limited lifespan that lasted only 550 ms. The phenomenon was presented in Fig. 5B.

We then simulated the formation of reentry arrhythmia in a 3D bi-ventricle model to mimic a more realistic situation. The normal sinus excitation wave was evoked by a series of sequential stimuli (S1) applied to the endocardium. The premature stimulus S2 of −104 pA/pF was applied to the upper region of the left ventricle when the refractory tail of S1 appeared. Similar to that in the 1D strand simulation, the S2 that applied during the vulnerable window led to a unidirectional conduction block. Simulation results are shown in Fig. 6. It can be observed that the unidirectional conduction block could be evoked in both wild-type and S755T mutation conditions after time delays of 360 and 250 ms separately from the previous S1 conditioning excitation wave. The earlier refractory tail in the S755T condition was an overall presentation of the shorter APDs of S755T mutation cells. The evoked unidirectional conduction block was evolved into scroll waves only in the mutation group, and these scroll waves were sustained throughout the whole simulation period of 5000 ms. In contrast, the scroll wave could not maintain in the wild-type situation due to its long wavelength. The wavefront caught up to the end of the refractory tail and self-terminated with a lifespan of less than 300 ms.

E. FREQUENCY DEPENDENCY ASSESSMENT OF THE FUNCTIONAL CONSEQUENCES OF THE S755T MUTATION

Above simulation results suggested that the S755T mutation caused cell-type-specific shortening of the APD and ERP, and consequently altered the vulnerability in tissues. However, this shortening was also expected to be frequency-dependent due to the restitution properties of cardiomyocytes. To access the frequency dependency of the functional consequences of the S755T mutation, the APD- and CV-restitutions, as well as the temporal susceptibility under different frequencies were investigated.

The APD- and CV restitution curves are plotted in Fig. 7. It can be observed in Fig. 7B that CV curves from different conditions were highly overlapped. This was attributed to the identical I_{Na} in all situations. For the APD restitution curves, it can be seen that the shortening of APD, measured as the gap between the paired two curves for wild-type and S755T conditions, was frequency-dependent and became smaller as DI decreased. To find out whether the different frequencies would cause different cell-type-specific shortening effects and lead to different conclusions from that determined under

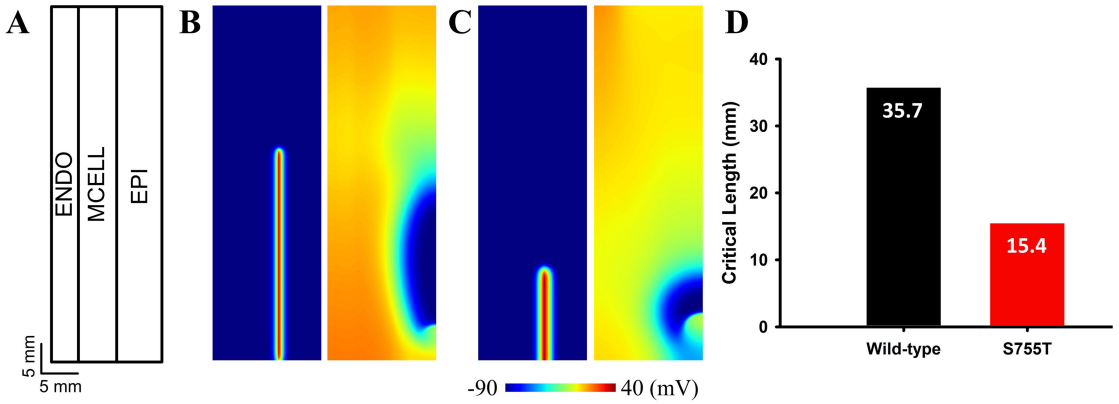

FIGURE 4. Simulation results of the critical length in the idealized 2D sheet. (A) The schematic diagram of the idealized 2D sheet. (B) The minimal length of S2 to provide a sufficient substrate for the formation of reentrant circuit in the wild-type tissue. (C) The minimal length in the tissue of SQTS6. (D) Comparison of the critical (minimal) length in the two situations.

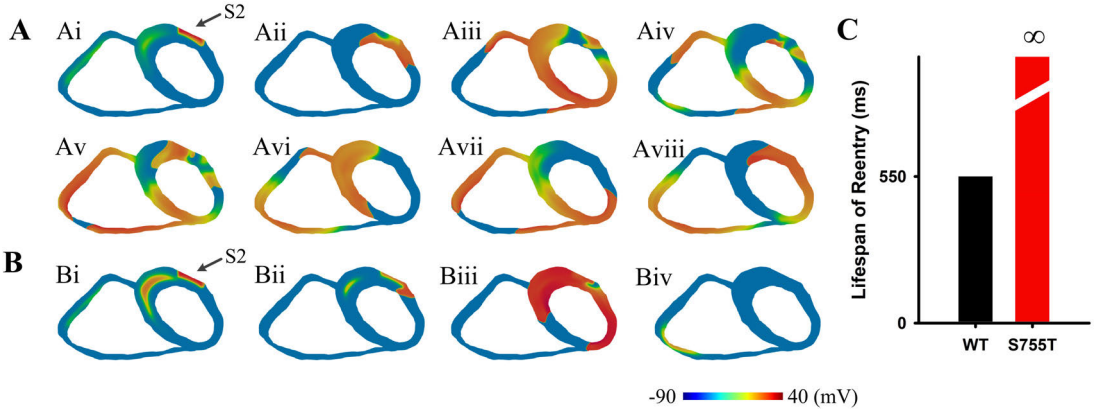

FIGURE 5. Simulation results of spiral waves in the realistic 2D ventricular slice. The locations of S2 stimulus were indicated by black arrows in Ai and Bi and were identical in both situations. (A) S755T mutation (SQTS6). Snapshots from Ai to Aviii were recorded at the time of 270, 320, 440, 520, 690, 820, 2000, 4000 ms. The spiral wave, as a type of functional reentry, transformed into anatomical reentry arrhythmia at about 820 ms and persisted since then. (B) Wild-type (control). Snapshots from Bi to Biv were recorded at the time of 380, 410, 510, 1000 ms. The evoked spiral wave could not sustain for one cycle and disappear after 1000 ms. (C) Lifespan of reentry in two situations.

1.25 Hz (i.e., BCL at 800 ms), four typical frequencies within the physiological range were chosen, and ΔAPD, ΔERP, and temporal vulnerable windows were calculated. The results are shown in Fig. 8 and Fig. 9. It can be observed in Fig. 8 that the transmural ΔAPD and ΔAPD in the S755T condition owned more flatted changes and was less frequency-dependent comparing with the wild-type condition, but the ΔAPD and ΔERP of the mutation condition was always smaller than its counterpart. Besides, no significant difference was found between MCELL-ENDO and MCELL-EPI. As for the VW, the average widths of VWs under different BCLs were all decreased in the S755T condition (see Fig. 9). In summary, the simulation results demonstrated that the functional consequences of the S755T mutation, including the decreased transmural dispersion of repolarization, and the decreased temporal vulnerability, were not frequency-dependent.

F. ROBUSTNESS ASSESSMENT OF THE FINDINGS

To evaluate the robustness of above findings, additional simulations were conducted using another human ventricular myocyte model, the O'Hara-Rudy dynamic (ORd) model. Detailed descriptions and results are presented in the *Supplementary Material*. Briefly, the simulation results suggested that the functional consequences of the S755T mutation were consistent in TNNP06 and ORd models. Therefore, the major findings including the abbreviated APD (Figure S1), the decreased ΔAPD and ΔERP (Figure S1), the decreased temporal vulnerability (Figure S2), and the increased spatial vulnerability (Figure S3), were robust and model independent.

IV. DISCUSSION

Short QT syndrome is a highly malignant cardiac disease. Although limited cases and families have been diagnosed worldwide, such lethal syndrome may be underdiagnosed [29]. Most cases were confirmed with identified life-threatening arrhythmias and family histories of SCD [3], [4]. In the present study, we utilized a multi-scale virtual heart to explore the arrhythmogenesis mechanisms in SQTS6 patients. Functional effects of the *CACNA1DC* S755T mutation on genesis and maintenance of ventricular

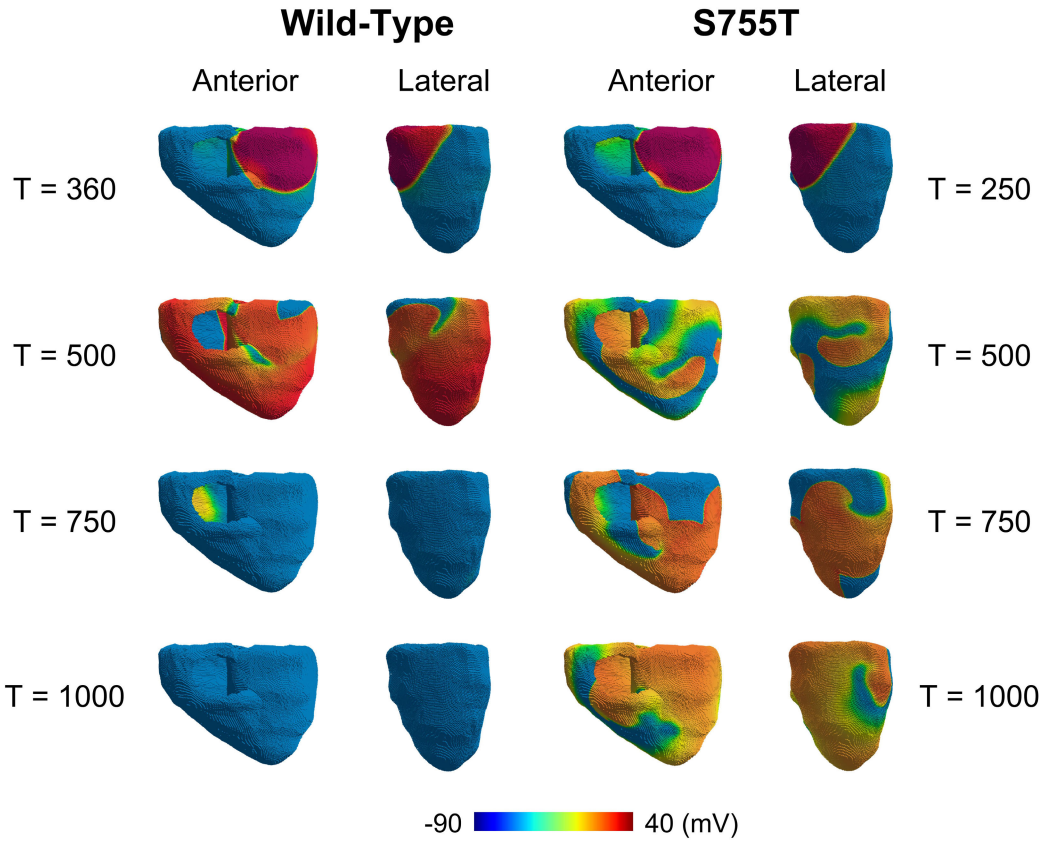

FIGURE 6. Simulation results of reentry arrhythmia in the realistic 3D bi-ventricle model. Left two columns are anterior and lateral views for wild-type, and right two columns for S755T. Snapshots were recorded at the time of 360/250(WT/S755T), 500, 750, 1000 ms. Noteworthy that scroll waves persisted throughout the whole simulation period of 5000 ms.

arrhythmias were thoroughly investigated. The main findings are summarized as follows: (i) APD and ERP were significantly abbreviated in the S755T mutation condition. This was attributed to the largely depressed I_{CaL} caused by the alteration of the $Ca_v\alpha_2\delta - 1$ subunit. The MCELL was the most affected type among the three cell types in the transmural ventricular wall; (ii) the unevenly reduced APD led to transmural heterogeneity remodeling. ΔAPD and ΔERP of adjacency cell types ($\Delta_{MCELL-ENDO}$, $\Delta_{MCELL-EPI}$) were reduced; (iii) simulation results of vulnerable windows using the 1D strand suggested that the S755T mutation decreased the temporal vulnerability; (iv) simulation results with the idealized 2D tissue revealed that the S755T mutation shortened the critical length for initiating reentry arrhythmia; therefore, patients with SQTS6 tend to have higher risks of developing reentry arrhythmias from a view of tissue spatial vulnerability; (v) simulation results from realistic 2D and 3D models demonstrated that the S755T mutation facilitated the maintenance of reentry. The evoked spiral waves (scroll waves) took the forms of either functional reentry or anatomical reentry and persisted in the S755T condition; (vi) the functional consequences of the S755T mutation were not frequency-dependent. The main simulation results were evaluated using two independent cell models, and the consistent results proved the robustness of the findings in this research. Taken together, the present study provided a comprehensive explanation about the mechanisms underlying the arrhythmogenesis in SQTS6, and substantiated the correlation between the gene mutation at the molecular level and the clinical characterization at the organ level.

The vulnerable window and the critical length provide appropriate quantitative indicators for evaluating the inducibility of arrhythmias, and the S1-S2 protocol is an imitation and reproduction of the arrhythmia initiation process in patients. Specifically, the S1 stimuli mimic the sinus rhythm, and the S2 represents the occurred extra- and ectopic beat in patients. For an ectopic trigger occurred in the ventricle, it does not always induce reentry arrhythmias. Instead, the trigger must occur during the VW, and requires a minimal size before it finally induces reentry arrhythmias. From a temporal perspective, the wider the vulnerable window, the more likely for an ectopic trigger to induce reentry arrhythmias. While from a spatial perspective, the shorter the critical length, the higher probabilities for an ectopic trigger to induce reentry arrhythmias. Therefore, the VW and the critical length offer quantitative measurements for

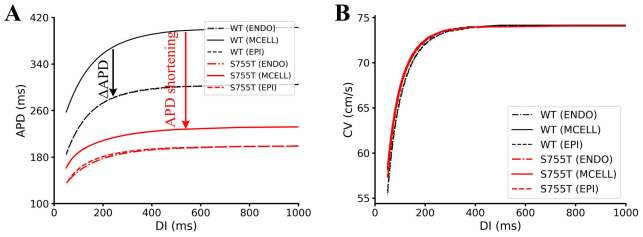

FIGURE 7. Restitution curves for wild-type and SQTS6 conditions. (A) APD restitution curve. (B) CV restitution curve.

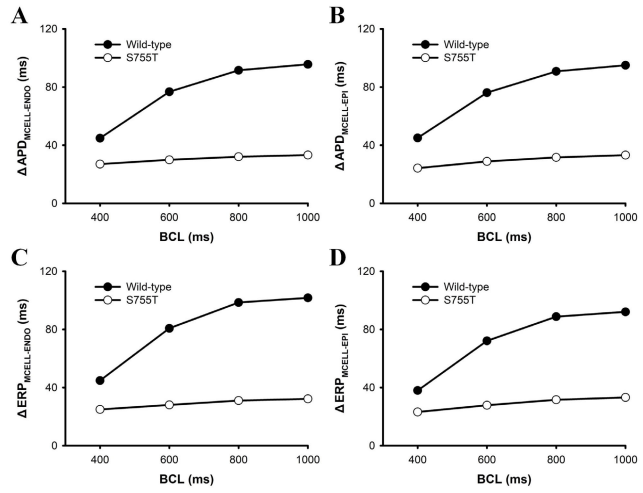

FIGURE 8. Frequency-dependency of ΔAPD and ΔERP in wild-type and S755T conditions. (A) $\Delta APD_{MCELL-ENDO}$ under different BCLs. (B) $\Delta APD_{MCELL-EPI}$ under different BCLs. (C) $\Delta ERP_{MCELL-ENDO}$ under different BCLs. (D) $\Delta ERP_{MCELL-EPI}$ under different BCLs.

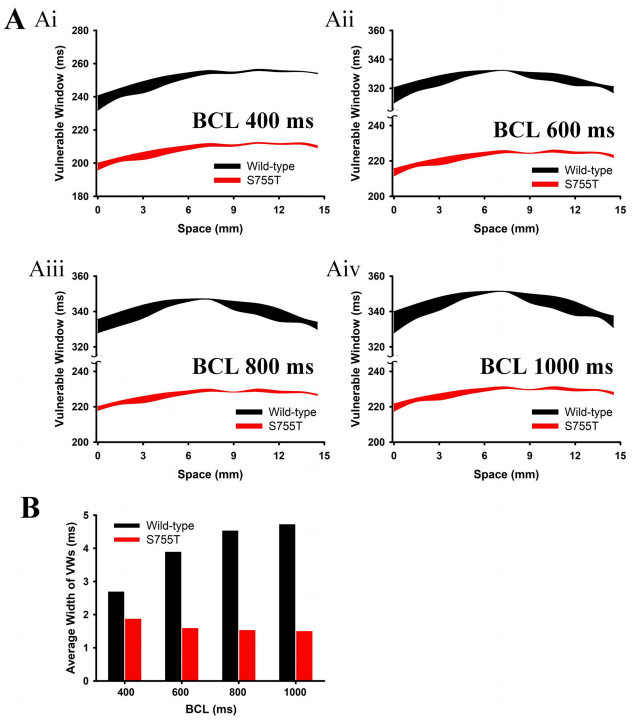

FIGURE 9. Vulnerable windows under different BCLs. (A) Distributions of VWs at BCLs from 400 ms to 1000 ms. (B) Comparisons of the average width of VWs in different conditions.

the inducibility of arrhythmias, and have been extensively adopted in other similar studies [20], [30].

It should be noted that the vulnerable window, as an indicator of the temporal vulnerability, was decreased in the mutation condition. The generally decreased temporal vulnerability was also reported in previous simulation studies regarding other SQTS variants [27]. This observation along with the attenuated APD and ERP dispersion were effects that actually anticipated to be anti-arrhythmic rather than pro-arrhythmic [27]. In this study, the decreased temporal vulnerability was a result of the decreased ΔAPD and ΔERP that generated by the uneven abbreviation of the AP repolarization phase in three cell types. The MID cell owned the longest APD, but was also most sensitive to the I_{CaL} depression among three cell types, therefore a same degree of I_{CaL} would lead to more decrements of APD of the MID cell comparing to that in EPI and ENDO cells, contributing to an accentuated transmural dispersion of repolarization and a decreased temporal vulnerability. An alternative hypothesis for the unexpected simulation results is that transmural heterogeneity might exist in the distribution of the affected $Ca_v\alpha_2\delta - 1$ subunit or the expression level of muted gene, for example, the altered $Ca_v\alpha_2\delta - 1$ subunit might be more abundant in EPI and ENDO cells albeit the identical calcium current density in all three cell types. Though the hypothesis has its plausibility, current experimental data are not sufficient to support more simulations. Therefore the hypothesis warrants more investigations in the future.

On the other hand, our simulation results clearly suggested that the S755T mutation resulted in a marked decrease in the minimal substrate size required for initiating and maintaining reentry arrhythmias. This highlights that both temporal and spatial vulnerability need to be evaluated to avoid biased conclusions and to understand the overall effects by mutations [31]. In the case of SQTS6, the increased spatial vulnerability in the mutation condition dominated, and eventually contributed to higher risks of developing arrhythmias in SQTS patients.

The main limitation of this study is the inconsistency between the simulated and the clinically observed ECGs (see Figure S4). Specifically, the model successfully reproduced the shortened QT interval that as a key characteristic pattern in the ECG from SQTS patients, however, it did not reproduce another important observation, i.e., the tall, narrow, and symmetric T-waves. Instead, the T-wave was flatted. This was due to the preferentially decreased APD in MID cells that contributing to an accentuated ΔAPD in the S755T mutation. The mechanism underlying such inconsistency remains to be further investigated. Based on available experimental data and current simulation results, the role of frequency can be excluded, as we have shown that the ΔAPD was decreased in physiologically relevant BCLs. The transmural heterogeneity

of I_{CaL} as another potential factor was also investigated. In this regard, the transmural heterogeneity of I_{CaL} that based on the experimental data of the expression of Cav1.2 [32] was incorporated into the TNNP06 model; however, a uniform reduction rate of I_{CaL} still failed to reproduce the tall T-wave in the strand of SQTS6 (data not shown). The APD of MCELL was still preferentially decreased in such settings. Considering the inconsistent T-wave pattern and the unexpected decrease of temporal vulnerability in current setting, we tried an uneven reduction ratio of I_{CaL} in different cell types based on the hypothesis that the muted gene is not equally expressed and the APD of EPI rather than MCELL is preferentially decreased. Specific model settings and model outputs are presented in the *Supplementary Material*. In this setting, the 1D model successfully reproduced the tall and narrow T-wave pattern as observed in patients. Noted that the preferentially decreased epicardial APD also suggested in an early research on SQTS1 [33]. Due to the lack of molecular or cellular evidences supporting the heterogeneous expression of the muted gene in different cell types, the simulation results based on uniformly decreased I_{CaL} were kept. More in-depth investigations are deserved before eventually unveiling the complete mechanisms for SQTS6.

The virtual heart model in this study can also act as a promising tool for screening potential drugs for SQTS6 in the future. Virtual heart models have been proved to be useful platforms for studying clinical cardiac arrhythmias [34] and screening drug cardiotoxicity [35], [36]. It is necessary to screen drugs according to the type of mutation, as the same drug does not have the same effect in different SQTS variants. For example, the Class Ia anti-arrhythmic drug disopyramide was shown to have a marked QT prolonging effect in SQTS1 but not in SQTS2 and SQTS3 [37]. In our case, as the ionic changes and pathological phenomena could be presented in great detail, the restoration degrees of APD and ERP, as well as that of the critical length may act as important indices for drug evaluation.

V. CONCLUSION

In this study, we found that the pro-arrhythmic factors of *CACNA1DC* S755T mutation mainly arise from an apparently decreased critical size needed for sustained reentry. Simulation results show that the significantly decreased I_{CaL} in the mutation condition led to abbreviated APD and ERP in all cell types. At the tissue level, the simulation revealed that the critical length for initiating reentry arrhythmia was shortened, and the evoked spiral waves persisted in the mutation condition but not in the control condition. The simulation results were evaluated under different frequencies and were assessed using two independent modes, and the consistent outputs suggested that the findings in this research was not frequency-dependent or model-dependent. These observations together indicate that the SQTS6 patients tend to be more vulnerable to the reentry arrhythmia. To sum up, the present study provides plausible explanation for how the gene mutation at the molecular level leads to the ventricular arrhythmia at the organ level in SQTS6 patients.

REFERENCES

[1] I. Gussak, "Idiopathic short QT interval: A new clinical syndrome?" *Cardiology*, vol. 94, no. 2, pp. 99–102, 2000.

[2] J. C. Hancox, D. G. Whittaker, C. Du, A. G. Stuart, and H. Zhang, "Emerging therapeutic targets in the short QT syndrome," *Expert Opinion Therapeutic Targets*, vol. 22, no. 5, pp. 439–451, May 2018.

[3] R. Brugada, K. Hong, R. Dumaine, J. Cordeiro, F. Gaita, M. Borggrefe, T. M. Menendez, J. Brugada, G. D. Pollevick, C. Wolpert, E. Burashnikov, K. Matsuo, Y. Sheng Wu, A. Guerchicoff, F. Bianchi, C. Giustetto, R. Schimpf, P. Brugada, and C. Antzelevitch, "Sudden death associated with short-QT syndrome linked to mutations in HERG," *Circulation*, vol. 109, no. 1, pp. 30–35, Jan. 2004.

[4] K. Hong, P. Bjerregaard, I. Gussak, and R. Brugada, "Short QT syndrome and atrial fibrillation caused by mutation in KCNH2," *J. Cardiovascular Electrophysiol.*, vol. 16, no. 4, pp. 394–396, Apr. 2005.

[5] C. Bellocq, A. C. G. van Ginneken, C. R. Bezzina, M. Alders, D. Escande, M. M. A. M. Mannens, I. Baró, and A. A. M. Wilde, "Mutation in the *KCNQ1* gene leading to the short QT-interval syndrome," *Circulation*, vol. 109, no. 20, pp. 2394–2397, May 2004.

[6] K. Hong, D. Piper, A. Diazvaldecantos, J. Brugada, A. Oliva, E. Burashnikov, J. Santosdesoto, J. Gruesomontero, E. Diazenfante, and P. Brugada, "De novo KCNQ1 mutation responsible for atrial fibrillation and short QT syndrome in utero," *Cardiovascular Res.*, vol. 68, no. 3, pp. 433–440, Dec. 2005.

[7] S. G. Priori, S. V. Pandit, I. Rivolta, O. Berenfeld, E. Ronchetti, A. Dhamoon, C. Napolitano, J. Anumonwo, M. R. di Barletta, S. Gudapakkam, G. Bosi, M. Stramba-Badiale, and J. Jalife, "A novel form of short QT syndrome (SQT3) is caused by a mutation in the KCNJ2 gene," *Circulat. Res.*, vol. 96, no. 7, pp. 800–807, Apr. 2005.

[8] C. Antzelevitch, "Loss-of-Function mutations in the cardiac calcium channel underlie a new clinical entity characterized by ST-segment elevation, short QT intervals, and sudden cardiac death," *Circulation*, vol. 115, no. 4, pp. 442–449, Jan. 2007.

[9] C. Templin, J.-R. Ghadri, J.-S. Rougier, A. Baumer, V. Kaplan, M. Albesa, H. Sticht, A. Rauch, C. Puleo, D. Hu, H. Barajas-Martinez, C. Antzelevitch, T. F. Luscher, H. Abriel, and F. Duru, "Identification of a novel loss-of-function calcium channel gene mutation in short QT syndrome (SQTS6)," *Eur. Heart J.*, vol. 32, no. 9, pp. 1077–1088, May 2011.

[10] K. Hong, J. Hu, J. Yu, and R. Brugada, "Concomitant brugada-like and short QT electrocardiogram linked to SCN5A mutation," *Eur. J. Human Genet.*, vol. 20, no. 11, pp. 1189–1192, Nov. 2012.

[11] K. Thorsen, V. S. Dam, K. Kjaer-Sorensen, L. N. Pedersen, V. A. Skeberdis, J. Jurevičius, R. Treinys, I. M. B. S. Petersen, M. S. Nielsen, C. Oxvig, J. P. Morth, V. V. Matchkov, C. Aalkjær, H. Bundgaard, and H. K. Jensen, "Loss-of-activity-mutation in the cardiac chloride-bicarbonate exchanger AE3 causes short QT syndrome," *Nature Commun.*, vol. 8, no. 1, pp. 1–10, Dec. 2017.

[12] Q. Zhang, J. Chen, Y. Qin, J. Wang, and L. Zhou, "Mutations in voltage-gated L-type calcium channel: Implications in cardiac arrhythmia," *Channels*, vol. 12, no. 1, pp. 201–218, Jan. 2018.

[13] C. Patel, G.-X. Yan, and C. Antzelevitch, "Short QT syndrome: From bench to bedside," *Circulat.: Arrhythmia Electrophysiol.*, vol. 3, no. 4, pp. 401–408, Aug. 2010.

[14] A. Mahajan, D. Sato, Y. Shiferaw, A. Baher, L.-H. Xie, R. Peralta, R. Olcese, A. Garfinkel, Z. Qu, and J. N. Weiss, "Modifying L-Type calcium current kinetics: Consequences for cardiac excitation and arrhythmia dynamics," *Biophys. J.*, vol. 94, no. 2, pp. 411–423, Jan. 2008.

[15] K. H. W. J. ten Tusscher and A. V. Panfilov, "Alternans and spiral breakup in a human ventricular tissue model," *Amer. J. Physiol.-Heart Circulatory Physiol.*, vol. 291, no. 3, pp. H1088–H1100, Sep. 2006.

[16] H. Zhang, T. Tao, S. Kharche, and S. M. Harrison, "Modelling changes in transmural propagation and susceptibility to arrhythmia induced by volatile anaesthetics in ventricular tissue," *J. Theor. Biol.*, vol. 257, no. 2, pp. 279–291, Mar. 2009.

[17] R. H. Clayton, O. Bernus, E. M. Cherry, H. Dierckx, F. H. Fenton, L. Mirabella, A. V. Panfilov, F. B. Sachse, G. Seemann, and H. Zhang, "Models of cardiac tissue electrophysiology: Progress, challenges and open questions," *Prog. Biophys. Mol. Biol.*, vol. 104, nos. 1–3, pp. 22–48, Jan. 2011.

[18] E. Drouin, F. Charpentier, C. Gauthier, K. Laurent, and H. Le Marec, "Electrophysiologic characteristics of cells spanning the left ventricular wall of human heart: Evidence for presence of m cells," *J. Amer. College Cardiol.*, vol. 26, no. 1, pp. 185–192, Jul. 1995.
[19] G.-X. Yan, W. Shimizu, and C. Antzelevitch, "Characteristics and distribution of m cells in arterially perfused canine left ventricular wedge preparations," *Circulation*, vol. 98, no. 18, pp. 1921–1927, Nov. 1998.
[20] D. G. Whittaker, H. Ni, A. P. Benson, J. C. Hancox, and H. Zhang, "Computational analysis of the mode of action of disopyramide and quinidine on hERG-linked short QT syndrome in human ventricles," *Frontiers Physiol.*, vol. 8, p. 759, Oct. 2017.
[21] P. Taggart, P. M. Sutton, T. Opthof, R. Coronel, R. Trimlett, W. Pugsley, and P. Kallis, "Inhomogeneous transmural conduction during early ischaemia in patients with coronary artery disease," *J. Mol. Cellular Cardiol.*, vol. 32, no. 4, pp. 621–630, Apr. 2000.
[22] G. Seemann, D. U. J. Keller, D. L. Weiss, and O. Dossel, "Modeling human ventricular geometry and fiber orientation based on diffusion tensor MRI," in *Proc. Comput. Cardiol.*, 2006, pp. 801–804.
[23] D. L. Weiss, D. U. J. Keller, G. Seemann, and O. Dössel, "The influence of fibre orientation, extracted from different segments of the human left ventricle, on the activation and repolarization sequence: A simulation study," *EP Europace*, vol. 9, no. 6, pp. vi96–vi104, Nov. 2007.
[24] M. A. Colman, M. Holmes, D. G. Whittaker, I. Jayasinghe, and A. P. Benson, "Multi-scale approaches for the simulation of cardiac electrophysiology: I—Sub-cellular and stochastic calcium dynamics from cell to organ," *Methods*, vol. 185, pp. 49–59, Jan. 2021.
[25] L. Dagum and R. Menon, "OpenMP: An industry standard API for shared-memory programming," *IEEE Comput. Sci. Eng.*, vol. 5, no. 1, pp. 46–55, 1998.
[26] Y. Xia, K. Wang, and H. Zhang, "Parallel optimization of 3D cardiac electrophysiological model using GPU," *Comput. Math. Methods Med.*, vol. 2015, Oct. 2015, Art. no. 862735.
[27] I. Adeniran, M. J. McPate, H. J. Witchel, J. C. Hancox, and H. Zhang, "Increased vulnerability of human ventricle to re-entrant excitation in hERG-linked variant 1 short QT syndrome," *PLoS Comput. Biol.*, vol. 7, no. 12, Dec. 2011, Art. no. e1002313.

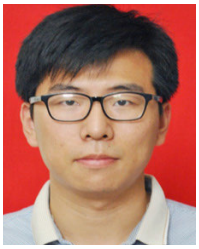

SHUGANG ZHANG received the Ph.D. degree in computer science from the Ocean University of China, in 2019. He was a Visiting Ph.D. Student with The University of Manchester, U.K., from 2017 to 2018. He is currently a Postdoctoral Researcher with the Department of Computer Science and Technology, Ocean University of China. His research interests include computational modeling of cardiac electrophysiology and *in silico* drug design with deep learning approaches.

WEIGANG LU received the Ph.D. degree in computer application technology from the Harbin Institute of Technology, China, in 2012. He is currently an Associate Professor with the Ocean University of China. His research interests include system modeling, scientific data visualization, and machine learning.

FEI YANG received the Ph.D. degree in computer science from the School of Computer Science and Technology, Harbin Institute of Technology, in 2012. From April 2010 to April 2011, he worked under the joint Ph.D. program with The University of Manchester. He is currently an Associate Professor with the School of Mechanical, Electrical and Information Engineering, Shandong University, Weihai. His current research interests include computer vision, scientific data visualization, and virtual organ modeling.

ZHIQIANG WEI received the Ph.D. degree from Tsinghua University, China, in 2001. He is currently a Professor with the Ocean University of China. He is also the Director of the Pilot National Laboratory, High-Performance Computing Center, Marine Science and Technology (Qingdao). His current research interests include intelligent information processing, social media, and big data analytics.